Experimental study on the globe thermometer behaviour in conditions of asymmetry of the radiant temperature

L. Fontana

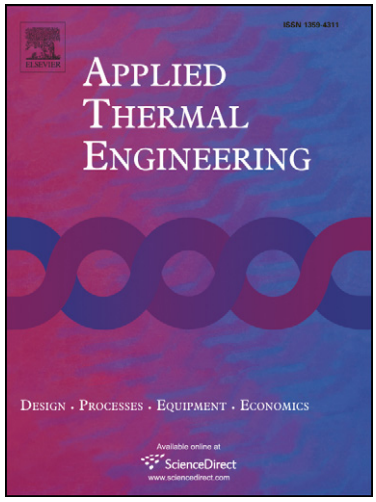

Experimental study on the globe thermometer behaviour in conditions of asymmetry of the radiant temperature

L. Fontana

PII: S1359-4311(09)00350-0
DOI: 10.1016/j.applthermaleng.2009.12.003
Reference: ATE 2940

To appear in: *Applied Thermal Engineering*

Received Date: 6 December 2007
Accepted Date: 3 December 2009

Please cite this article as: L. Fontana, Experimental study on the globe thermometer behaviour in conditions of asymmetry of the radiant temperature, *Applied Thermal Engineering* (2009), doi: 10.1016/j.applthermaleng.2009.12.003

EXPERIMENTAL STUDY ON THE GLOBE THERMOMETER BEHAVIOUR IN CONDITIONS OF ASYMMETRY OF THE RADIANT TEMPERATURE

*L. Fontana**

Dipsa - Dipartimento di Progettazione e Studio dell'Architettura

Università degli Studi di Roma Tre

Piazza della Repubblica 10, Rome, Italy

**corresponding author* lfontana@uniroma3.it phone: 00393475403858

Abstract

Heating and cooling systems based on the use of hot or cold floors or ceilings meet increasing favour. In such systems, moreover, radiant temperature gains a far greater importance than in traditional systems; and therefore the importance of measurement and control techniques grow; but at the same time, in presence of these systems, unavoidably the radiant field tends to become asymmetrical.

In this work a theoretical study and an experimental check on the most common radiant temperature measurement tool, the globe thermometer, when used in conditions of asymmetrical radiant temperature are described. The results point out the necessity of a more complete definition of the features of the globe thermometers designed to operate in non symmetric radiative fields, especially with reference to covering material and thickness, to temperature sensor position and to radiative properties of the inner surface.

Keywords Globe thermometer, Radiant temperature, Asymmetry

Nomenclature

a	absorption coefficient
A	area
A_{PV}, A_{PH}, A_T	projected vertical area; projected horizontal area; total area (of the ellipsoid)
A_{LB}, A_{UB}, A_{SS}	area of the lower bottom; area of the upper bottom; area of the side shell, (relative to a cylindrical globe thermometer)
A_{FLOOR}	Area of the floor surface
A_{CEY}	Area of the ceiling
A_{SIDE}	Area of the side walls
C_P	constant pressure specific heat
$F_{dA_1 dA_2}$	view factor of dA_2 from dA_1
$f(...)$	general function symbol
h	local convection coefficient
h_{CE}	coefficient of convection on the outer surface of the globe thermometer
h_{RO}	coefficient of radiation on the outer surface of the globe thermometer

h_{RI}	coefficient of radiation on the internal surface of the globe thermometer
H	cylinder height
L	radiosity (radiant energy outcoming for unit surface)
E	radiant energy incoming for unit surface
q	specific heat flux
q_{CONV}	convective specific heat flux
q_{RAD}	radiative specific heat flux
R	cylinder radius
Ra	Rayleigh number $Ra = Gr \cdot Pr = \frac{\beta g (t - t_A) H^3 \rho^2}{\mu^2} \cdot \frac{c_P \mu}{\lambda} = \frac{\beta g (t - t_A) H^3 \rho^2 c_P}{\mu \lambda}$
r	radial coordinate
s	thickness
T	absolute temperature, K
t	centigrade temperature, °C
t_{RT}, $T_{R\,T}$	mean radiant temperature (centigrade, absolute) "seen" by the top surface of the cylindrical globe thermometer
t_{RB}, T_{RB}	mean radiant temperature (centigrade, absolute) "seen" by the bottom surface of the cylindrical globe thermometer
t_{RS}, T_{RS}	mean radiant temperature (centigrade, absolute) "seen" by the side surface of the cylindrical globe thermometer
t_{UB}, T_{UB}	temperature (centigrade, absolute) in the upper bottom of the cylindrical globe thermometer
t_{LB}, T_{LB}	temperature (centigrade, absolute) in the lower surface of the cylindrical globe thermometer
t_{SS}, T_{SS}	temperature (centigrade, absolute) in the side surface of the cylindrical globe thermometer
t_A	temperature of the external air
t_{TOP}	mean radiant temperature (experimental) "seen" by the top surface of the cylindrical globe thermometer
t_{BOTTOM}	mean radiant temperature (experimental) "seen" by the bottom surface of the cylindrical globe thermometer
t_{SIDE}	mean radiant temperature (experimental) "seen" by the side surface of the cylindrical globe thermometer
t_{CEY}	average temperature of the ceiling
t_{FLOOR}	average temperature of the floor
t_{SIDE}	average temperature of the side walls
t_{AIR}	air temperature (experimental) at the center of the globe thermometer
u	radial velocity
v	axial velocity
z	axial coordinate

Greek Symbols

η	emissivity
β	expansion coefficient
λ	thermal conductivity
μ	dynamic viscosity
ρ	specific mass
σ	Stefan-Boltzman constant

Subscripts

1	referred to the current surface element
2	referred to the surface element "seen" by the current element
o	referred to the black body
R	radiant (referred to the temperature)
SAV	surface average

Superscripts

R	referred to the radiant energy
G	referred to the experimental globe thermometer
T	result of the theoretical model

1. Introduction

Heating and cooling systems based on the use of hot or cold floors or ceilings are getting increasingly popular. In such systems moreover, radiative exchanges and radiant temperature gain greater importance than in traditional systems; the importance of measurement and control techniques of these properties grows accordingly; but at the same time, the radiative field tends to become asymmetrical.

Globe thermometer is the most common radiant temperature measurement tool. The methodologies so far suggested (e.g. the European Standard EN 27726-1993 [1]) to deduce the mean radiant temperature from the globe temperature, stand on the assumption that the temperature at the center of the globe is equal to the average temperature of the globe surface. The presence of non uniformity and asymmetry of the radiant temperature, causes non-uniformity of the globe surface temperature, which in turn brings non-uniformity of the globe internal air temperature and consequently internal convective flows could arise: in particular the temperature value in the center of the globe could be different from any average of the surface temperatures, resulting in errors in average radiant temperature computations.

Aim of this work is an investigation on such theme.

2. Previous works and Standard references.

Since H.M. Vernon first proposed the usage of globe thermometer as a measurements tool for radiative heat exchanges between human bodies and environment [2], the interest in such a device has developed in multiple directions. On one side, the target has been to build a tool able to simulate the human body

reactions to environmental conditions, so as to obtain a complete thermal environment meter. In this direction the papers by Bedford e Warner [3], Botsford, [4] and later Kuehn et al. [5], who proposed devices sensitive to air humidity as well; Madsen [6], who proposed a tool that could simulate the human body answer to sensible heat exchanges, based on a human thermo-regulation model grounded on the Fanger theories; and eventually Mendes e Da Silva [7], who more recently proposed a device that could simulate the human body reactions to both sensible and latent heat exchanges.

On the other side, the globe thermometer has been further studied and perfectioned as a mean radiant temperature measurement tool. Research has meanly focused on topics such as accuracy [8,9], promptness of results [10,11], optimization of shape and size [9,12,13]. Though the influence of radiative field non uniformity on comfort conditions is relevant and deeply investigated [14, 15, 16], it was not possible to find papers dedicated to the behaviour of the globe thermometer itself in highly asymmetrical conditions; in particular, it is worthwhile investigating weather or not such conditions may cause measurements inaccuracies. This deficiency is present as well in standardization initiatives, that do ignore such problems.

The current standards [1], with reference to radiant temperature measurement, give only the following essential definitions, prescriptions or instructions.

2.1. Shape of the globe thermometer

In appendix B the mentioned Standard suggests as best approximation of the shape of a standing human body, with reference to the view factors between the body itself and the various environment walls, a rotation solid (e.g. ellipsoid) with assigned values of the projected area factors (ratio between projected surface and total surface) equal to 0.08 for the vertical projection (A_{PV} / A_T), and 0.28 for the horizontal (A_{PH} / A_T) projection. Those two ratios are not independent from each other in the rotation ellipsoid.

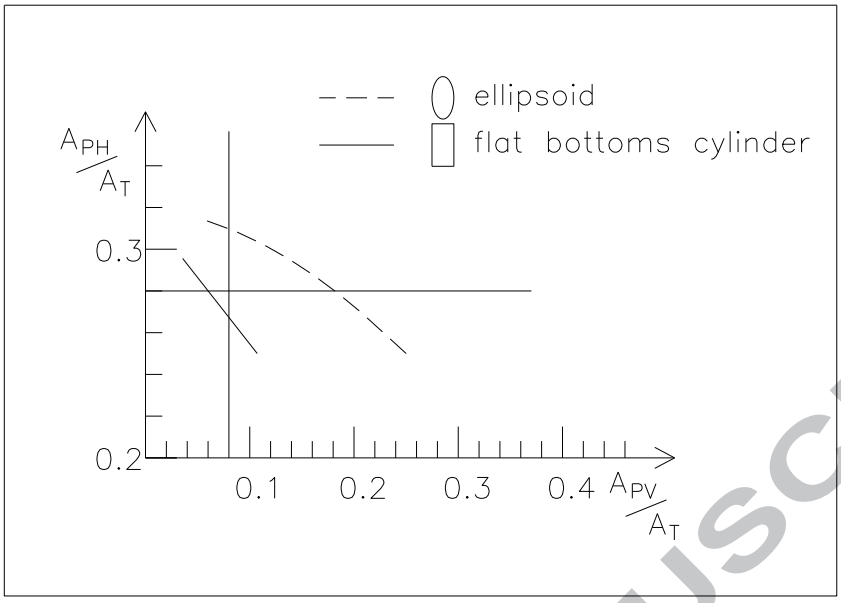

Figure 1. Projected area ratios for the ellipsoid and cylinder with flat bottoms

In Fig. 1 the A_{PV} / A_T ratio value versus the A_{PH} / A_T ratio value is reported for the rotation ellipsoid and the simplest shape to be studied and realized, the cylinder with flat bottom surfaces. It appears that the two specifications suggested by the Standard (A_{PV} / A_T =0.08 and A_{PH} / A_T =0.28) are jointly respected by the cylinder with better approximation than the ellipsoid. For these reasons, this investigation has been referred to the cylindrical with flat bottoms shape.

2.2. Construction features

In Appendix B of the Standard the globe thermometer is described as a "black globe with a temperature sensor placed in the middle". A diameter not below 15cm is suggested, and the blackening of the outer surface of the globe is required, so as to realize emissivity values close to 0.95. A small thickness of the covering is recommended. No other constructive requirement is given about material to be used, internal emissivity, thickness , thermal conductivity of the covering.

3. Theoretical study

In a previous work [17] a theoretical study has been conducted, on the free convection inside a cavity with thin conductive covering, subject to convective and radiative thermal exchanges both on the outer and the inner surface.

Reference has been made to a cylindrical cavity with flat bottoms, for different values of the height to diameter ratio, placed vertically in a room with uniform air temperature and dissymmetry of the radiant temperature.

More precisely, it was supposed that:

- Each point of the upper bottom outside surface "sees" the same average temperature T_{RT}, and each point of the lower bottom outside surface "sees" the same average temperature T_{RB};
- Each point of the side surface "sees" the same radiant temperature, assumed equal to $T_{RS} = \frac{T_{RT} + T_{RB}}{2}$.

With reference to the interior surface of the globe, it was supposed that:

- The surface has a grey and Lambertian behaviour.
- The fluid-dynamic field has axial symmetry.
- The expected maximum values of the Rayleigh number Ra turn out equal to about 6×10^6. The flow has been therefore considered as laminar.

3.1. *The mathematical model*

The thermo-fluid-dynamic field inside the globe is described by the Navier-Stokes energy and continuity equations, with reference to a Boussinesq fluid (constant fluid properties except for the density in the buoyancy terms), laminar flow, cylindrical coordinates (r,z) and steady state.

The model is therefore described by the following equations:

Momentum according to *r:*
$$u\frac{\partial u}{\partial r} + v\frac{\partial u}{\partial z} = \frac{1}{\rho}\frac{\partial p}{\partial r} + \frac{\mu}{\rho}\left(\frac{\partial^2 u}{\partial r^2} + \frac{1}{r}\frac{\partial u}{\partial r} - \frac{u}{r^2} + \frac{\partial^2 u}{\partial z^2}\right) \quad (1a)$$

Momentum according to z:
$$u\frac{\partial v}{\partial r} + v\frac{\partial v}{\partial z} = \frac{1}{\rho}\frac{\partial p}{\partial z} + \frac{\mu}{\rho}\left(\frac{\partial^2 v}{\partial r^2} + \frac{1}{r}\frac{\partial v}{\partial r} - \frac{u}{r^2} + \frac{\partial^2 v}{\partial z^2}\right) + \rho g \quad (1b)$$

Continuity:
$$\frac{\partial u}{\partial r} + \frac{u}{r} + \frac{\partial v}{\partial z} = 0 \quad (2)$$

Energy:
$$u\frac{\partial t}{\partial r} + v\frac{\partial t}{\partial z} = \frac{1}{\rho}\frac{\partial p}{\partial r} + \frac{\lambda}{\rho c_P}\left[\frac{1}{r}\frac{\partial}{\partial r}\left(r\frac{\partial t}{\partial r}\right) + \frac{\partial^2 t}{\partial z^2}\right] \quad (3)$$

The 1st type boundary conditions are:

On the bottom surfaces $0 \le r \le R$: $t(r,0) = f_0(r)$; $\quad t(r,H) = f_H(r)$

On the side surface $0 \le z \le H$: $\quad t(R,z) = f_R(z)$ (4)

The thermal field inside the covering is described in the hypothesis of negligible temperature changes through the thickness. Moreover, in the hypothesis of axial symmetry, the thermal field turns out to be one-dimensional, function of z in the side shell and of r in the two bottoms. The heat transfer through the covering slab is by conduction; on the two slab surfaces the convection and radiation heat exchanges are taken into account.

The thermal field is therefore described by the equations:

lower bottom:
$$\lambda s\left(\frac{d^2 t_{LB}}{dr^2} + \frac{1}{r}\frac{dt_{LB}}{dr}\right) = \left[h_{CE}(t_{LB} - t_A) + \sigma_0 \eta (T_{LB}^4 - T_{RB}^4)\right] + q_{CONV} + q_{RAD} \quad (5)$$

upper bottom:

$$\lambda s\left(\frac{d^2 t_{UB}}{dr^2}+\frac{1}{r}\frac{dt_{UB}}{dr}\right)=\left[h_{CE}\left(t_{UB}-t_A\right)+\sigma_0\eta\left(T_{UB}^4-T_{RT}^4\right)\right]+q_{CONV}+q_{RAD} \quad (6)$$

shell:

$$\lambda s\frac{d^2 t_{SS}}{dz^2}=\left[h_{CE}\left(t_{SS}-t_A\right)+\sigma_0\eta\left(T_{SS}^4-T_{RS}^4\right)\right]+q_{CONV}+q_{RAD} \quad (7)$$

and for each portion of the covering the boundary conditions are given by the temperature continuity.

In the (5-7) q_{CONV} is the convective specific heat flux (outgoing) exchanged between the current surface element and the air inside the globe; q_{RAD} is the net specific heat flux (outgoing) from the current surface element resulting from the radiative exchanges balance with the inner surface of the globe. The flux q_{RAD} is evaluated with the radiosity method, in the hypotheses of grey and Lambertian behaviour for emission and reflection.

With the notations shown in Nomenclature, and being dA_1 the current surface element; dA_2 any internal surface element "seen" from dA_1; T, L and E the absolute temperature, the radiosity and the specific radiative incoming flux of dA_2, the radiative balance for the generic element dA_1 is given by

$$E dA_1=\int_S L\cdot dA_2\cdot F_{dA2\,dA1} \quad (8)$$

where S is the globe thermometer inner surface, and furthermore

$$L=E(1-a)+\sigma_0 a T^4; \qquad q_{RAD}=\sigma_0 a T^4-E\cdot a \quad (9)$$

The numerical investigation has been conducted studying two extreme cases: the black body ($\eta\cong 1$, simulating an inner surface painted with a high emissivity paint), and absence of radiative exchanges ($\eta\cong 0$, bare and bright metal inner surface).

The thermal and fluid-dynamic field in the air and the conductive field in the covering are matched through the q_{CONV}, t_{UB}, t_{LB}, t_{SS} variables. More precisely the system solution has been obtained by iteration. In any iteration, q_{CONV} values were determined by the inner field, being valid the relations

upper bottom: $q_{CONV}=-\left(-\lambda\frac{\partial t}{\partial z}\right)_{z=H}$; *lower bottom:* $q_{CONV}=-\lambda\frac{\partial t}{\partial z}\Big|_{z=0}$;

side shell: $q_{CONV}=-\left(-\lambda\frac{\partial t}{\partial r}\right)_{r=R}$; (10)

with such values the thermal field is solved in the covering. The obtained temperatures act as boundary conditions for the thermal field in the inner air assuming:

$$t_{LB}(r)\equiv f_0(r); \qquad t_{UB}(r)\equiv f_H(r); \qquad t_{SS}(r)\equiv f_R(z) \quad (11)$$

The procedure is iterated up to convergence.

3.2. Numerical solution

The set of governing equations (1-7 and 10-11) has been solved through a control-volume formulation of the finite-difference method. A monomial interpolation scheme ("power-law") has been used for the diffusive-convective terms. The pressure-velocity coupling through the continuity equation is handled by the SIMPLE algorithm described in detail by Patankar [18].

The resultant algebraic equation system has been solved iteratively, line by line, with the Thomas algorithm. The non linear coefficients have been iteratively replaced with the dated values, applying under-relaxation criteria. The integration domain has been covered by a grid with uniform mesh-spacings except close the borders where the mesh was finer. The solution is considered to be fully converged when the maximum absolute values of both the mass source and the percent changes of the dependent variables at any grid-node from iteration to iteration are smaller than prescribed values, i.e., 10^{-4} and 10^{-6}, respectively.

For every height to diameter ratio, the dependence of the obtained results from the mesh pacing has been tested. Grids have been examined increasing by a pace of 3 the mesh number in the integration domain. Then grid-size values representing a good compromise between solution accuracy and computational time required, were assumed as those over which further grid refinements did not produce material modifications (i.e. 0.1%) in the heat transfer rates and in the maximum and minimum shell temperature values. The used typical grid was therefore of about 21x21 meshes for the square configuration, and 18x27 for the slim.

The system of (8, 9) that expresses the radiative exchanges among elements of the internal surface has been expressed in discrete terms as well, with reference to plane concentric rings for the bottoms and circular cylindrical surfaces for the shell. Values of the view factors have been calculated by the relations in closed form available in any view-factors catalog, e.g. in [19].

4. Results of the theoretical model

The results are showed in Fig.2 through the values of the ratio Θ/Θ_R where Θ is the difference between the highest and the lower values of the shell temperature, and Θ_R is the difference among the extreme values assumed for the radiant temperature ($\Theta_R = t_{RB} - t_{RT}$). The Θ/Θ_R values are reported as a function of ($\lambda \cdot s$), assuming the other relevant variables (H, R, η) as parameters.

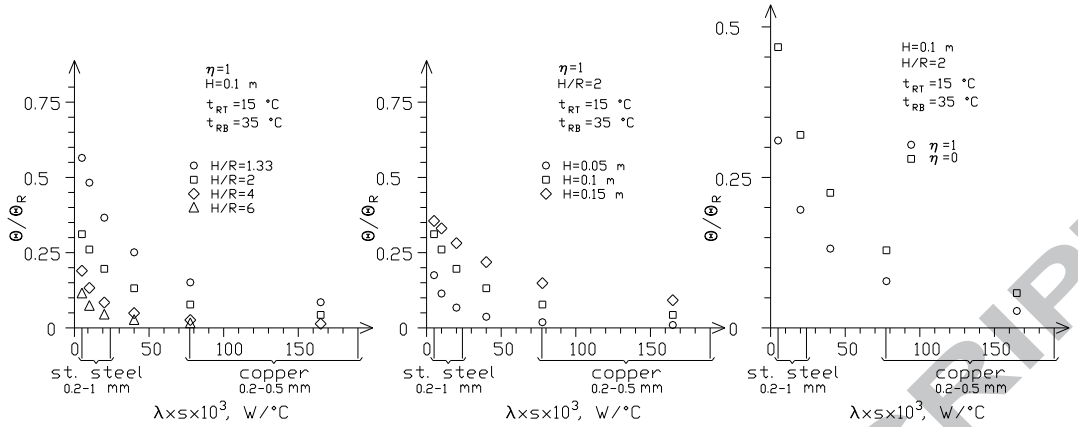

a) **b)** **c)**

Figure 2. Results of the theoretical model

a) Θ/Θ_R **, vs.** $\lambda \cdot s$ **, for several H/R values and H=0.1 m;**

b) Θ/Θ_R **, vs.** $\lambda \cdot s$ **, for several values of H and H/R = 2;**

c) Θ/Θ_R **, vs.** $\lambda \cdot s$ **, for** η **=0 or** η **=1, with H = 0.1 m and H/R = 2.**

Results show that, for some variable combinations, the temperature non-uniformity can turn out to be important, with Θ/Θ_R values up to 0.5. The non-uniformity increases as the product $\lambda \cdot s$ decreases, as H grows and as H/R ratio decreases.

For $\lambda \cdot s$ typical values for stainless steel ($5 \div 25 \cdot 10^{-3}$ W/°C), with the dimensions required from the Standard (H = 15 cm), and the ratio H/R = 2 (the examined shape nearest to the spherical one), Θ/Θ_R values between 0.25 and 0.3 in case of black internal surface, and between 0.4 and 0.6 in absence of radiative internal exchanges, have been obtained. That means, with Θ_R values of about 20 °C (it is the case in presence of a radiant floor), a globe surface temperature unevenness of about 10 °C. The situation is completely different in case of globe thermometers made of copper, ($\lambda \cdot s = 78 \div 385 \cdot 10^{-3}$ W/m): the ratio Θ/Θ_R takes values of about 0.05 for black inner surface and 0.1 in absence of radiative heat exchanges (corresponding to a surface temperature non uniformity of about 1 or 2 °C in the cited conditions).

The inner air temperature is moreover measured in the globe thermometer. The maximum non-uniformity of the air temperature inside the globe is equal to that of the covering, but the convective flows could attenuate it in the central zone, far from the walls. So the inner temperature measured in presence of a such surface temperature non uniformity could not correspond to the mean temperature of the shell surface; and therefore the radiant temperature value, obtained from the inner globe thermometer temperature measure, could be affected by an error.

The obtained fluid-dynamic fields can give an idea of the above, within the limits given by the hypothesis of axial symmetry.

In Fig. 3 some of the recurring configurations are showed. One or more frequently two superimposed recirculating cells appear, often moreover of non regular and different shape.

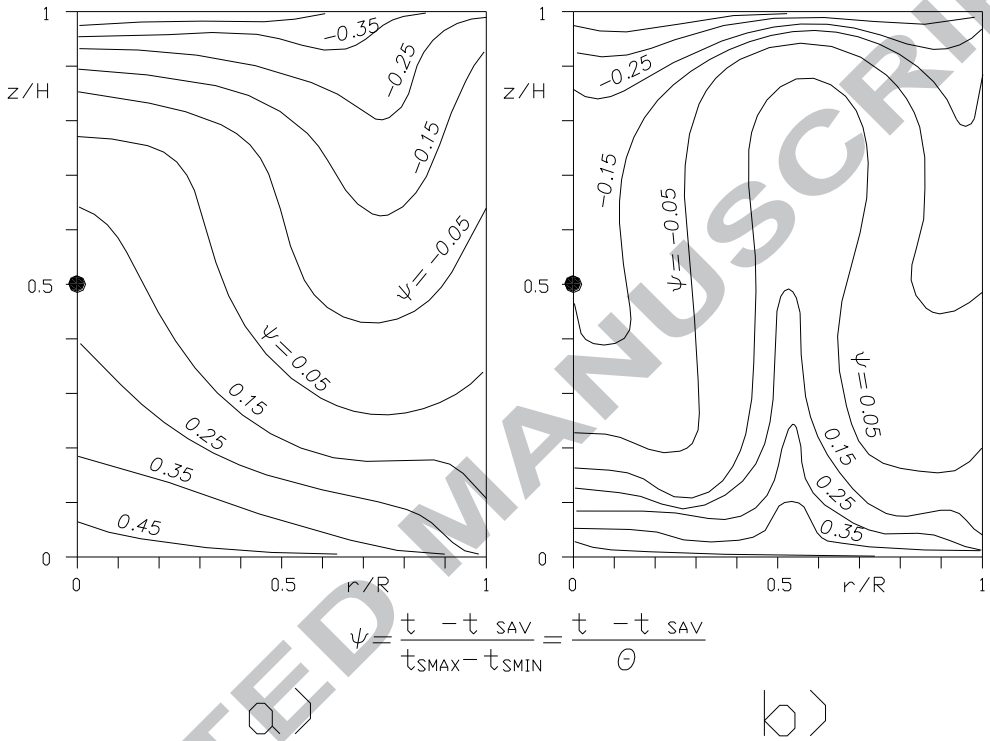

Figure 3. Examples of the inner thermal fields

a) H=0.05m; R=0.0375m; s=0.25mm; λ=20W/mK

b) H=0.1m; R=0.075m; s=0.25mm; λ=20W/mK

Differences from some hundredth to same tenth of Θ are observed between the air temperature evaluated in the cylinder center and the surface average temperature of the globe, with a maximum of about 2°C in the examined conditions. For distances of about R/5 from the center the difference increases, up to 50%.

Therefore it would seem favourable to make the temperature measurement strictly at the center of globe thermometer.

This behaviour moreover could turn out different in presence of geometrically different asymmetries of the radiant temperature, and cylinder positions other than vertical; this is a matter of the experimental study. Vice versa, the obtained results suggest that small enough non-uniformities may however be obtained:

- Realizing the covering in copper or silver and among 0.5 mm - 1mm thick.
- Using high-emissivity paints in the inner surface. Any not-electrically conductive paint could in practice be adopted, while it appears important not to leave naked the inner metal surface.
- Not exceeding the dimension (15 cm) suggested by the Standard; strictly referring to the the surface non-uniformities, smaller dimension (about 10 cm) would be preferable.

5. Experimental study

Two cylindrical globe thermometers, one made of iron and one made of copper and a scale model of the indoor space, equipped for surface and air temperature measurement and control, have been realized as below described.

5.1. The environment model

A scale model (box shaped) has been realized, as sketched in Fig. 4.

The model scale dimensions, albeit small compared with the globe thermometer dimension, do not materially influence the convection heat transfer coefficients over the external globe surface.

All the relations in use and suggested by the standards e.g. [1] to deduce the mean radiant temperature from the globe temperature are referred to free convection in still air, and do not take into account possible convection flows on a large scale, that could differ between the model and the real room scale, the latter being higher.

On the other hand, the globe thermometer gives reliable results when used in absence of significant convection flows (other than those due to the globe itself).

Besides, both the thermo-fluid-dynamic fields over the globe surface and on the model walls surfaces are of the boundary layer type, with thickness below 1 cm. In the model the distance between the globe thermometer and the wall surfaces is always bigger than 13 cm, so the boundary layers over the globe external surface and over the walls surfaces are far and do not interfere.

In these conditions, the convection coefficient h_{CE} depends on the globe height H, that in the experimental model has been kept of the size suggested by the standards and of the commonly used globe thermometers, and on the difference between globe surface and air temperatures, that in the experimental test has been set on values comparable with the real ones.

The walls and the ceiling have been made using 0.5 cm plywood sheets, and a 2 cm layer of expanded polystyrene.

The surface temperatures are measured through 10 K-type thermocouples applied to each wall (Fig. 5).

Two additional K-type thermocouple, with polished joint, placed respectively at the level of the upper and lower bottom of the globe thermometer, and at a distance of 5 cm from the globe thermometer side surface, measure the inner air temperature.

A small fan equipped with an electrical heater lets an air flow of up to 7 vol/h, properly heated, be introduced in the box. This option has only been used for the globe thermometers calibration, as shown in section 5.2.

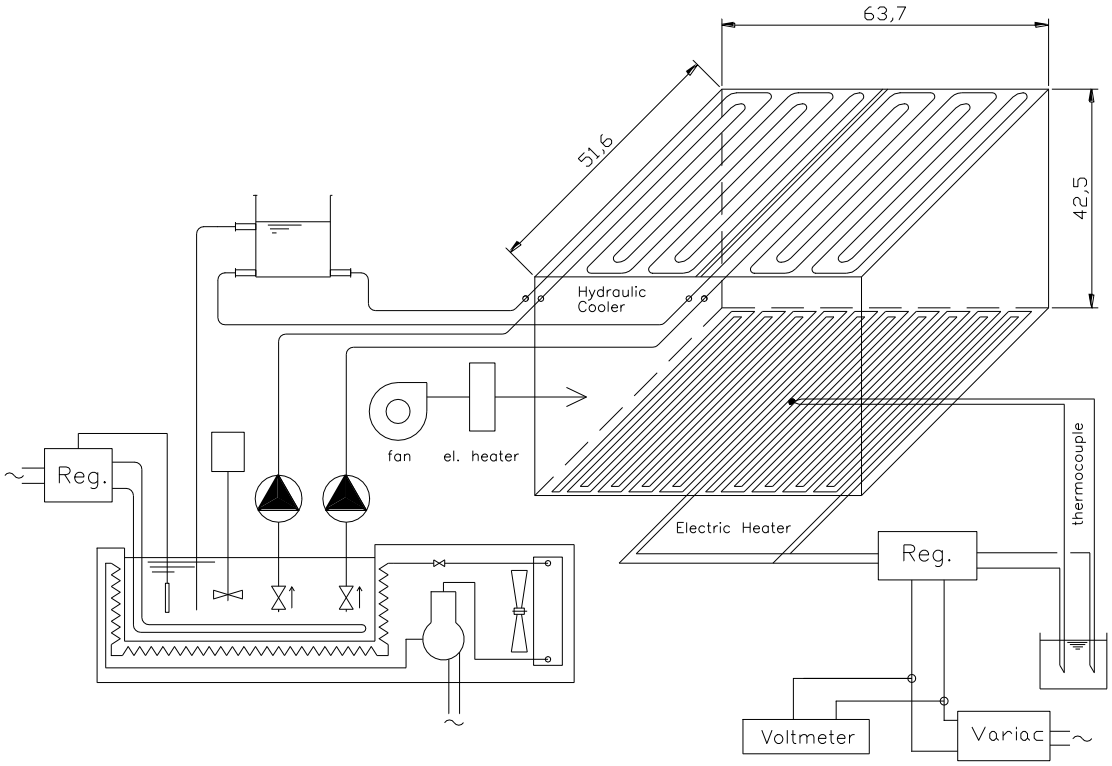

Figure 4. Sketch of the scale model (dimensions in cm) with the electrical feeding of the heating floor and the hydraulic feeding of the cold ceiling

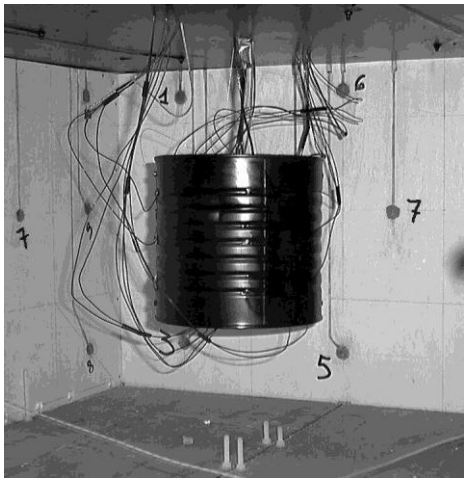

Figure 5. Arrangement of the globe thermometer and the thermocouples on the walls inside the box

5.1.1 Heating floor

The heated floor is made of a nylon slab under which an heating element is inserted. Between the heating element and the nylon slab a copper sheet 0.5mm thick has been placed, in order to reduce the surface temperature non uniformity. The heater is electrically supplied by an autotransformer. On the upper nylon slab surface 16 K-type thermocouples have been applied.

A further thermocouple is inserted on the center of the upper surface. The signal of such thermocouple has been used for the floor thermal control; a temperature control within +-0.2 °C has been obtained. In the experimental study temperature in the range between 33°C and 55°C have been set.

The thermocouples applied to the walls and the floor are made up using wires 0.2 mm diameter. In order to minimize the thermal field perturbation produced by the thermocouple insertion, the wires run on the surface for length of various hundreds of diameters and the joint is stuck to the wall with an interposed disk of copper 0.2 mm thick and diameter 15 mm, as recommended in [20].

5.1.2. Cold ceiling

The ceiling is realized in two equal parts, each made by a panel refrigerated by a cold fluid circulation.

The cold-water hydraulic circuit is embedded in a epoxy resin slab 6 mm thick, placed between two aluminium sheets 0.8 mm thick.

The hydraulic circuit is formed by a polyethylene pipe (external diameter 6 mm, internal 4 mm), disposed in plane-coil with going and return pipes running side by side (Fig. 4), so that the average couple temperature remains constant for the length of the coil.

To improve the ceiling temperature uniformity, a single aluminium slab 1.5 mm thick, having the ceiling dimensions, has been applied to the lower face of the two panels. Such slab is the ceiling surface; it has

been painted with several black paint coats, and has been equipped with six thermocouples. A slab of expanded polystyrene 25 mm thick and a panel of plywood 6 mm thick have been stuck to the upper side.

5.1.3. Ceiling feeding and thermal control system

In the coil embedded in the ceiling panels flows a forced circulation of a water (60%) and ethil alcohols solution, refrigerated by a chiller. The required cooling power is of a small number of watt. Since a chiller of a so little power production doesn't exist, it was obtained from a modified domestic ice-cream-maker, as shown in Fig. 4.

A temperature control within +-0.2 °C has been obtained inserting in the pool of the cold solution an electrical heater regulated by a thermostat, equipped with a Pt100 type thermometer. The temperature values of the incoming water flow into the ceiling have been set at 8-14°C; the temperature difference between inlet and outlet/entrance and exit was of about 2-3 °C, thus obtaining ceiling surface temperature values between 10°C and 15°C.

5.2. Globe thermometers

Two cylindrical globe thermometers (15 cm diameter, 15 cm height) have been realized, with different materials; one has been realized with a mild steel sheet, the other with a copper sheet, both 0.4 mm thick. Thermocouples have been arranged both on the covering and inside.

In both cases the thermocouples on the covering were of the so-called "intrinsic" type: for each thermocouple one of the two components was the covering material; the other one was formed by constantan wires (diameter 0.25 mm, with silicone insulation, all from the same spool). Therefore the thermocouples were iron-constantan in a case, and copper-constantan in the other.

In both cases, a thermocouple was realized with a thin strip of the metal sheet used for the covering, and a constantan wire from the above mentioned spool; such thermocouples have been submitted to careful calibration in the range 0÷100 °C.

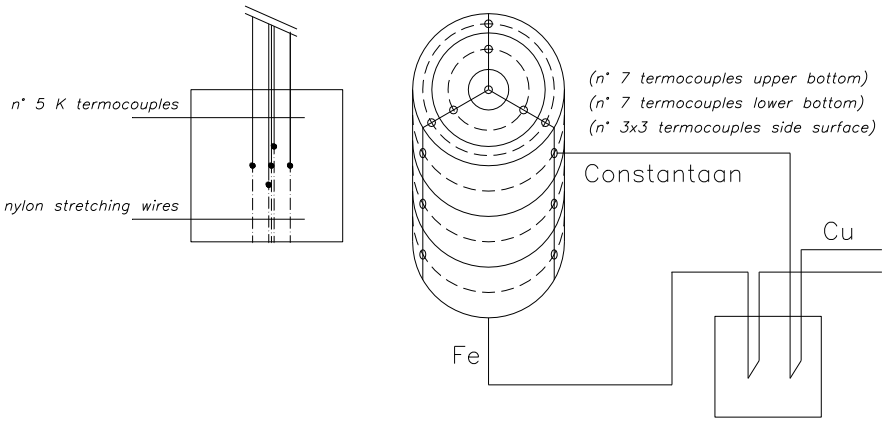

Figure 6. Thermocouples arrangement inside and on the covering of the globe thermometer

Thermocouples on the side surface have been placed on three lines at a 120 degrees angular distance, and on each line, in three positions (1/6, 1/2 and 5/6 of the cylinder height).

Each bottom was ideally shared in three zones of equal area, a circle and two circular crowns. The thermocouples have been placed in the center of the circle and along three radial lines, on the circumferences which share the circular-crown zones in two parts of equal area.

Fig. 5,6 show the globe in the box, the thermocouple arrangement and the measurement circuit scheme.

Five inner thermocouples have been placed in an axial plan; one in the geometrical cylinder center, the others in four points distant 1.5 cm from the center and both in the parallel and normal directions to the cylinder axis. The K-type thermocouples have been realized with wires (0,2 mm diameter) arranged so as to be kept in tension and to ensure a good positioning and alignment of the thermocouples.

For each globe thermometer, different series of measurements have been done, with the internal surface naked and emery, or painted with two black paint coats.

Globe thermometers have been calibrated determining the globe temperature (temperature t_{AIR}^{G} measured by the thermocouple in the centre of the cylinder) in conditions such that both the floor heating system and the ceiling cooling one were inactive while a hot air flow was introduced. In such conditions the side walls, the floor and the ceiling were all at very close temperatures –and so in absence of asymmetry- but different from the environment air temperature of about 10°C.

The mean radiant temperature, obtained from the walls surfaces temperature measurements as described in 5.3, has then been compared with the mean radiant temperature value deducted from the globe

temperature with the relations given in the Standard [1]. The two values were in accordance in the range ±0,25°C.

6. Measurements and results – Comparison with the theoretical model

Measures of all the temperatures have been made for three different values of the floor temperature set up. For the chilled water the outlet temperature of 10 °C has been always set up. In such conditions it was not produced moisture condensation on the ceiling surface.

From the temperature values of the walls surfaces and of the globe thermometer surface, we have derived the:

– Average temperature t_{CEY} of the ceiling, t_{FLOOR} of the floor and t_{SIDE} of the side walls. Ceiling, floor and walls have been ideally divided into portions of ΔA_K area; in each portion centre the K thermocouple was placed. Then $t_{FLOOR} = \frac{1}{A_{FLOOR}} \sum_{A_{FLOOR}} \Delta A_K t_K$ and so on.

– Mean radiant temperature (°C) respectively "seen" by the top bottom of the globe thermometer (t^R_{TOP}), by the lower bottom (t^R_{BOT}) and by the side shell (t^R_{SIDE}) with:

$$t^R_{TOP} = \left(\sum_{A_{WALLS}} (t_K + 273.16)^4 F_{S_{TOP} \to \Delta A_K} \right)^{.0.25} - 273.16$$

where $A_{WALLS} = A_{FLOOR} + A_{CEY} + A_{SIDE}$ and furthermore $F_{S_{TOP} \to \Delta A_K}$ is the factor of view of the ΔA_K surface sight from the surface of the upper bottom, and so on.

– Maximum and minimum values of the globe thermometer surface temperature t^G_{MAX}, t^G_{MIN}.

– Air temperature values inside the enclosure in the two described positions, t_{A1}, t_{A2}.

– Surface average temperature of the globe thermometer t^G_{SAV}. The globe thermometer surface S_G has been ideally divided into portions ΔS_K, and in the geometrical center of each portion the thermocouples were placed. Then $t^G_{SAV} = \frac{1}{S_G} \sum_{S_G} \Delta S_K t_K$.

– Air Temperature value at the center of globe thermometer, t^G_{AIR}.

The view factors have been numerically computed. Each ΔA_K surface has been divided in smaller portions δAK_j (average dimension roughly 3 cm) and the temperature measured in the centre of ΔA_K has been attributed to each of them. Similarly, the various cylinder surfaces have been divided in $\delta A1_i$ portions. A

cartesian coordinate system has been assumed as in Fig. 7, then the general formula as proposed in [10] has been used. For instance, to compute the t_{TOP}^{R}:

$$F_{S_{TOP}\Delta A_K} = \frac{1}{S_{TOP}} \sum_i \sum_j \delta A1_i \delta AK_j \frac{[(x_{Kj} - x_{1i})l_{1i} + (y_{Ki} - y_{1i})m_{1i}(z_{Kj} - z_{1i})n_{1i}] \cdot [(x_{1i} - x_{Kj})l_{Kj} + (y_{1i} - y_{Kj})m_{Kj}(z_{1i} - z_{Kj})n_{Kj}]}{R^3}$$

where:

$$R = [(x_{Kj} - x_{1i})^2 + (y_{Kk} - y_{1i})^2 + (z_{Kj} - z_{1i})^2]^{1/2}$$

and l,m,n are the direction cosines of the local surface perpendicular lines.

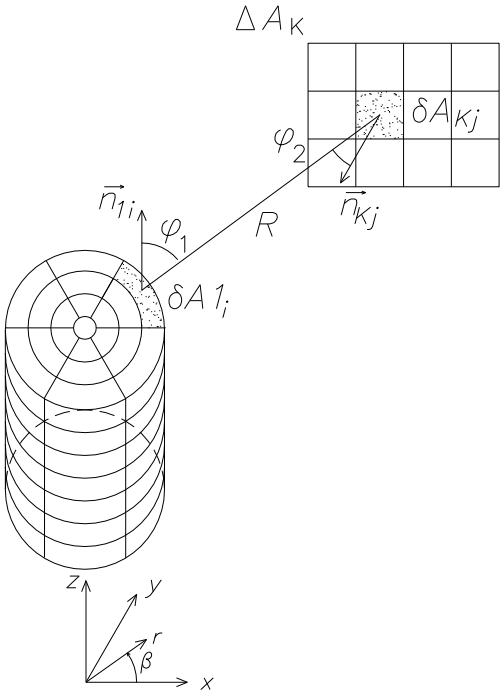

Figure 7. The surface subdivision

The obtained values are shown in Tab. I.

	t_{CEY} °C	t_{FLOOR} °C	t_{SIDE} °C	t_{A1} °C	t_{A2} °C	t^{R}_{TOP} °C	t^{R}_{BOT} °C	t^{R}_{SIDE} °C	t^{G}_{MAX} °C	t^{G}_{MIN} °C	t^{G}_{SAV} °C	t^{G}_{AIR} °C
Iron,black	10.9	33.8	22.3	22.5	22.4	12.5	33.2	22.9	24.8	20.2	22.4	22.0
	13.0	41.0	25.7	26.3	26.6	15.1	40.4	26.9	29.6	24.1	26.5	26.1
	14.1	52.0	30.7	31.8	31.8	16.8	51.3	32.5	36.5	28.9	32.1	31.5
Iron, metal bright	12.3	34.2	23.1	23.4	22.9	14.1	33.8	23.7	25.9	21.0	23.2	23.0
	13.1	41.8	26.2	26.9	26.6	15.2	41.4	27.4	30.5	24.0	26.8	26.5
	15.1	51.6	30.9	31.9	31.9	17.7	51.0	32.7	36.8	28.6	32.0	31.5
Copper,black	11.2	34.1	22.7	22.7	22.6	13.2	33.5	23.2	24.0	22.4	23.2	23.1
	13.0	41.6	25.8	26.5	26.7	15.1	40.6	27.0	28.3	26.1	27.3	27.1
	14.5	51.8	30.6	31.8	31.8	17.0	51.2	32.5	34.4	31.4	33.0	32.8
Copper, metal bright	12.2	34.3	23.2	23.3	23.0	14.0	33.8	23.7	24.5	22.8	23.7	23.6
	13.1	41.9	26.2	27.0	26.8	15.2	41.5	27.5	29.3	26.1	27.8	27.7
	15.3	51.7	30.7	32.0	32.0	17.8	51.1	32.7	34.9	31.7	33.4	33.2

Tab. I Experimental results

Lastly, to compare the experimental results with the theoretical model, for T_{RT}, T_{RB} and T_{RS}, we have assumed to use respectively the values t^{R}_{TOP}, t^{R}_{BOT} e t^{R}_{SIDE} obtained in the experimental session, and assuming the appropriate values of λ, η, s and of the other variables involved. More precisely it has been assumed:

- η = 0.95 for the internal enclosure surfaces and the globe thermometer outer surfaces; for the internal globe thermometer surface, it has been assumed, η = 0.15 for the naked surface and η = 0.95 for the painted surface.
- λ = 55 W/m°C for the iron; λ = 385 W/m°C for the copper
- s = 0.4 mm for both the iron and the copper.

Fig. 8a) shows the experimental values of (t^{G}_{MAX} - t^{G}_{MIN}) and the values obtained in the same conditions, from the theoretical model. Fig. 8b), as an example, shows the same comparison between measured globe thermometer surface temperatures and the values obtained with the numerical model.

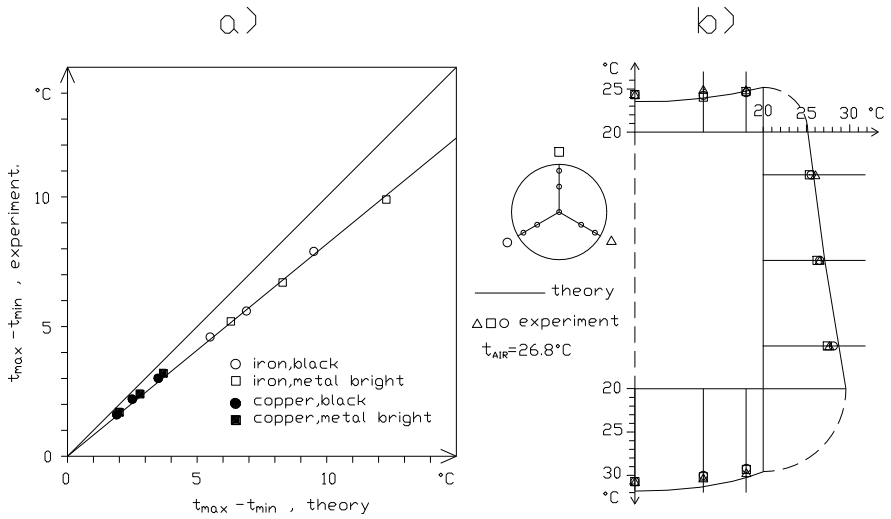

Fig. 8 Theoretical and experimental results:

a) t_{MAX}-t_{MIN} values

b) Surface temperatures -iron- naked inner surface. t_{FLOOR} = 41.8 °C; t_{CEY} = 13.1 °C; t_{AIR} = 26.7 °C

Tab. II shows, for the iron globe thermometer and for different values of t_{FLOOR} and t_{CEY}, the values of the air temperature inside the globe thermometer (measured in five points as above described and shown in fig. 6), compared with the corresponding theoretical value. Lastly, Tab. III, for the various realized values of t_{FLOOR} and t_{CEY} , shows values of t_{AIR}^{G} obtained in case of vertical or tilted globe thermometer.

	t_{CEY} °C	t_{FLOOR} °C	$t^G_{UNDER} \backslash t^T_{UNDER}$ °C	$t^G_{AIR} \backslash t^T_{AIR}$ °C	$t^G_{OVER} \backslash t^T_{OVER}$ °C	$t^G_{SIDE1} \backslash t^T_{SIDE}$ °C	t^G_{SIDE2} °C
Iron,black	10.9	33.8	22.2\22.8	22.0\22.5	21.9\22.4	22.1\22.2	22.2
	13.0	41.0	26.2\26.7	26.2\26.5	25.9\26.4	26.3\26.1	26.2
	14.1	52.0	31.7\32.4	31.5\32.2	31.3\32	31.8\31.5	31,7
Iron, metal bright	12.3	34.2	23.2\23.7	23.0\23.4	22.8\23.1	23.1\23.2	23.0
	13.1	41.8	26.6\27.7	26.5\27.0	26.2\26.8	26.6\26.7	26.6
	15.1	51.6	31.7\35.6	31.5\34.8	31.3\34	31.8\33.2	31.6

Tab. II Comparison between the experimental and the theoretical results –air temperature values-

Iron globe thermometer

	T_{CEY} °C	T_{FLOOR} °C	t^G_{SAV} °C, Globe upright	t^G_{AIR} °C, Globe upright	t^G_{SAV} °C, Globe tilted	t^G_{AIR} °C, Globe tilted
Iron,black	≈11	≈34	22.4	22.0	22.2	21.9
	≈13	≈41	26.5	26.1	25.8	25.4
	≈15	≈52	32.1	31.5	31	30.4
Iron, metal bright	≈12	≈34	23.2	23.0	22.0	21.6
	≈13	≈41	26.8	26.5	25.3	24.9
	≈15	≈52	32.0	31.5	29.5	29

Tab.III. Case of vertical or tilted Iron globe thermometer

With reference to the globe thermometer surface temperature values, the experimental results confirm the predictions of the theoretical model and, in particular for the values of $t^G_{MAX} - t^G_{MIN}$, there is a fairly good agreement. The experimental values turn out lower (about 20%) than those given by the model; the trend of Fig. 8 b) shows that deviations are correlated (with reference both to the magnitude and the sign) to the difference between the surface temperature and the air temperature. This behaviour and the deviations magnitude are in accordance with the effect of "extended surface" caused by the thermocouples, evaluated as in [20].

Referring to the air temperature values, the differences between air temperature at the center of the globe thermometer and surface average temperature are of the same order as the theoretical ones. The

experimental values of the difference between the side and the centre values of the air temperature also appear to be close to the theoretical ones. Significant differences among the vertical and the inclined globe thermometer do not result.

7. Conclusions

The radiant temperature measurement is based on the assumption that the temperature at the center of the globe is equal to the average temperature of the globe surface. This assumption could be not verified in presence of non-uniformity of the radiant temperature, that could cause a globe thermometer surface temperature non–uniformity, with consequent growing convective flows inside the globe and temperature value in the center of the globe different from any average of the surface temperatures.

The study has pointed out the advisability of a more complete definition of the features of globe thermometers designed to work in radiative non uniform and asymmetric environments: particularly, the importance of thermal conductivity of the material used, covering thickness, temperature sensor position, inner surface radiative properties has been pointed out.

The experimental study has confirmed the reliability of the theoretical model, within the accuracy limits expected.

The theoretical model shows, in accordance with the experimental results, that the circulation of internal air can produce in the central zone an attenuation of non-uniformity and an alignment of the air temperature value to the surface average temperature value; however, the results of this study show that the difference between the air temperature value in the centre of the globe and the globe surface average temperature, could bring errors of some centigrade degrees °C in the radiant temperature measurement. In the case, for example, of a globe thermometer with a thin stainless steel covering (λ=20 W/m°C, thickness s= 0.25 mm) this error can achieve 2°C, and could be much bigger in the case of globe thermometers made of plastic as proposed in [13].

However, the results also show that with simple constructive precautions (copper covering, thickness not lower than 0.5 mm, internal high-emissive surface) the surface temperature unevenness can be reduced to negligible values, and the related radiant temperature measurement error become unimportant.

REFERENCES

[1] EN 27726 “Thermal Environments - Instruments and methods for measuring physical quantities", 1993. UNI EN ISO 7726 “Ergonomics of the Thermal Environment - Instruments for measuring physical quantities", 2002.

[2] H.M. Vernon, The measurement of radiant heat in relation to human comfort, Journal of Industrial Hygiene 14 (1932) 95-111.

[3] T. Bedford, C.G. Warner, The globe Thermometer in studies of heating and ventilation, Journal of Hygiene, 4 (1934) 458-473.

[4] J.H. Botsford, A wet globe thermometer for environmental heat measurement, American Industrial Hygiene Association Journal, 32 (1971) 1-10.

[5] L.A Kuehn, R.A Stubbs, L.E. Mac Hattie, A single thermometer wet bulb globe temperature index meter, Journal of Physics E: Scientific Instruments, 4 (1971) 293-295.

[6] T.L. Madsen, A new instrument for measuring thermal confort, Proc. 5th Int. Congress for Heating,Ventilating and Air-Conditioning, 1971.

[7] JCAF Mendes, M.C. Gameiro da Silva, Development of a new thermal environment meter responding both to sensible and latent heat fluxes, Measurement Science and Technology, 15 (2004) 839-847.

[8] E.N. Hey, Small Globe Thermometers, Journal of Scientific instruments, 1 (9) (1968) 955-957.

[9] K.W. Graves, Globe Thermometer evaluation, American Industrial Hygiene Association Journal 35 (1) (1974) 30-40.

[10] G.Eissing, I. Steinhaus, Investigation and Improvement of the Adjustment time of the Globe thermometers, Klima, Kalte, Heizung, 10 (3) (1982) 103-115.

[11] M. Nikolopoulou, N. Baker, K.Steemers, Improvements to the globe thermometer for outdoor use. Architectural Science Review, 42 (1) (1999) 27-34.

[12] M.A. Humpreys, The optimum diameter for a globe thermometer for use indoors, Annals of Occupational Hygiene, 20 (2) (1977) 135-140.

[13] R. De Dear, Ping-Pong Globe Thermometers For Mean Radiant Temperatures, H&V Engineer, 60 (681) (1988) 10-11.

[14] P.O. Fanger, Thermal Confort, Mc Graw-Hill, N.Y.

[15] E. Kahkonen, Draught, radiant temperature asymmetry and air temperature – a Comparison between Measured and Estimated Thermal Parameters, Indoor Air 1(4) (1991) 439-447.

[16] Tomonori Sakoi, Kazuyo Tsuzuki, Shinsuke Kato, Ryozo Oaka, Doosam Song, Shengwei Zhu, Thermal confort, skin temperature distribution, and sensible heat loss distribution in the sitting posture in various asymmetric radiant fields, Building and Environment, 42 (12) (2007), 3984-3999.

[17] L.Fontana, Studio sul comportamento di globotermometri in condizioni di asimmetria della temperatura radiante, Proceedings of the LX ATI National Congress, Associazione Termotecnica Italiana, Roma, September 2005.

[18] S.V. Patankar, Numerical Heat transfer and fluid flow, Jon Benjamins Publishing Co., 1980.

[19] M.F. Modest, Radiative Heat Transfer, MC Graw-Hill, Inc. N.Y., 1993.

[20] M. Jacob, Heat Transfer, John Wiley &Sons, New York, 1957. 151-159.